Sensors and Materials, Vol. 30, No. 10 (2018) 2171–2181
MYU Tokyo

S & M 1667

Linear Variable Differential Transformer Temperature Compensation Technique

Wandee Petchmaneelumka,* Pitsini Mano, and Vanchai Riewruja

Department of Instrumentation and Control Engineering, Faculty of Engineering,
King Mongkut's Institute of Technology Ladkrabang, Bangkok 10520, Thailand

(Received November 27, 2017; accepted March 12, 2018)

Keywords: LVDT, temperature compensation, inductive transducer, analog circuit design

A feedback technique to compensate for the temperature effect on the output signal of the linear variable differential transformer (LVDT) without losing the sensitivity is presented in this paper. The proposed technique is based on the use of a voltage-controlled amplifier to scale the amplitude of the excitation signal for temperature compensation. The proposed feedback technique provides the proportional-plus-integral control action to minimize the error caused by the temperature variation. The proportional-plus-integral action is realized using the integral scheme in the proposed technique. The peak amplitude of the LVDT output signal is sampled by the sample-and-hold circuit (SHC) to obtain the feedback and displacement signals, where the control signal of the SHC is provided by the LVDT output signal. The proposed LVDT temperature compensation technique is emphasized in terms of simple configuration and low cost. Note that the proposed technique is suitable for signal conditioners embedded in smart sensors and smart materials. The performance of the proposed technique is confirmed by experimental implementation using commercially available devices. The maximum error of the core displacement signal can be reduced from 6.52% for the uncompensated scheme to 0.098% for the compensated scheme at the ambient temperature of 70 °C.

1. Introduction

The linear variable differential transformer (LVDT) is an inductive transducer that is widely applied in instrumentation and measurement systems. The LVDT provides the behavior in terms of high resolution, high linearity, and durability, and is employed for measuring the displacement. The applications of the LVDT can be found in the fields of industries, military, vehicles, structural health monitoring, and scientific and medical equipment for the measurement of position, level, force, flow, and pressure.[1–6] The LVDT consists of a primary winding and two secondary windings connected in series with opposite directions similar to a transformer. The moving core of the LVDT is used for sensing the displacement. The output signal of the LVDT is subtracted between the two secondary windings in the form of amplitude modulation with suppressed carrier (AMSC). Previously, the phase-sensitive

*Corresponding author: e-mail: wandee.pe@kmitl.ac.th
https://doi.org/10.18494/SAM.2018.1816

ISSN 0914-4935

demodulator formed by a diode and a low-pass filter was used to demodulate the displacement signal from the LVDT signal. The disadvantage of this method is that the large error due to the threshold voltage of the diode occurs.[1] To overcome this error, the analog multiplier and low-pass filter formed as the synchronous demodulator can demodulate the displacement signal without a diode in the signal path. The use of a low-pass filter in traditional approaches deteriorates the response time and stability of the demodulator. Recently, the use of a sample-and-hold circuit (SHC) instead of the analog multiplier and low-pass filter in the synchronous demodulator is more attracted.[7–12] The SHC provides the transfer characteristic in terms of the 'sinc' function, the behavior of which is close to an ideal low-pass filter.[13] Thus, the use of the SHC in the synchronous demodulator can remove the high-frequency components of the LVDT signal to achieve the displacement signal without disturbing the performance of the demodulator. The reference frequency used for the synchronous demodulators mentioned above is provided by the excitation signal. Practically, the phase shift between the excitation signal and the LVDT signal occurs owing to the structure of the LVDT. This phase shift causes the error in the demodulated signal. In addition, the output signal of the LVDT can also be interfered by the variation in ambient temperature. The aforementioned approaches are achieved only with the demodulator without temperature compensation. Therefore, the applications of the LVDT for a high-temperature environment are avoided. There are two recent approaches using dual secondary windings in the LVDT structure for the compensation of the temperature effect.[14,15] Unfortunately, both approaches require a specific design of the LVDT structure; such approaches are unsuitable for commercial purposes. Alternately, the approach based on the ratiometric technique has been proposed.[16] This approach requires the analog multiplier, the analog divider, and the synchronous demodulator, which deteriorates the response time and system stability. In addition, the aforementioned approaches are unsuitable for embedded systems and smart sensors used in a smart factory owing to the complicated topology of the signal conditioner. In this paper, the proposed feedback technique is introduced for the minimization of the temperature effect. The feedback signal is provided by the sum of two secondary winding signals, which obtains a constant amplitude signal. The proposed feedback scheme provides a proportional-plus-integral control action to reduce the error due to the ambient temperature variation. Moreover, the error caused by the phase shift is prevented because the reference frequency is directly achieved from the secondary winding signals. The proposed scheme is attractive in terms of simple configuration and low cost.

2. Circuit Description

The simplified diagram of the LVDT is depicted in the dash-line block of Fig. 1(a). The LVDT output signal is obtained from the difference between two secondary winding signals. If the signal $v_{ex} = V_P \sin\omega_{ex}t$ is applied to the primary winding, where $\omega_{ex} = 2\pi f_{ex}$ and f_{ex} is the excitation frequency, then the two secondary winding signals v_{S1} and v_{S2} can be written as

$$v_{S1} = K_L l_C \left(1 + \frac{l}{l_C}\right)(1 - \alpha\Delta T) V_P \sin(\omega_{ex}t + \phi_S), \tag{1a}$$

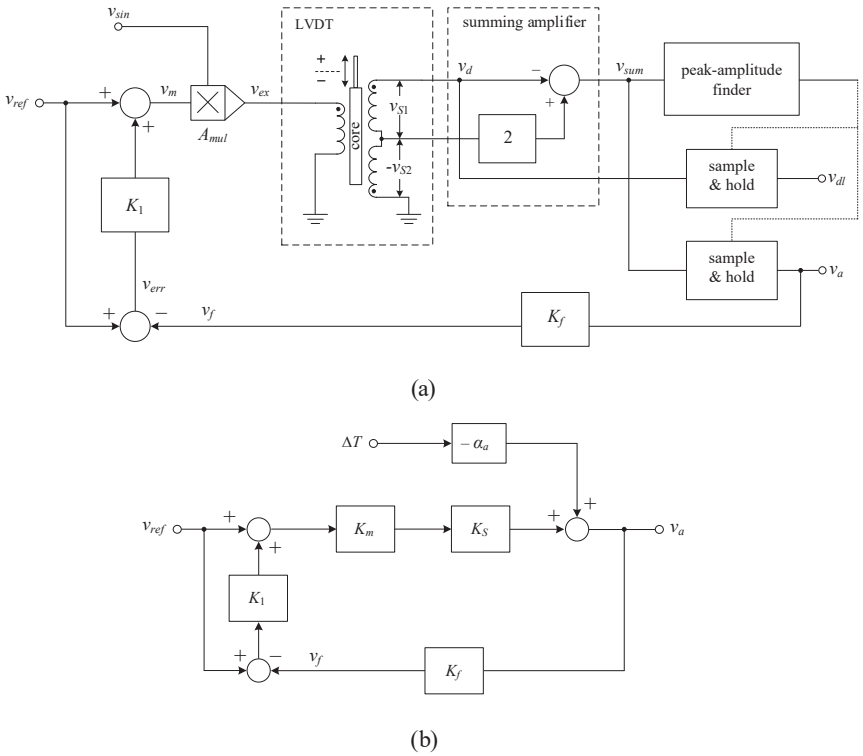

Fig. 1. (a) Principle of proposed technique and (b) block diagram.

$$v_{S2} = K_L l_C (1 - \frac{l}{l_C})(1 - \alpha\Delta T) V_P \sin(\omega_{ex} t + \phi_S), \tag{1b}$$

where K_L is the sensitivity of the LVDT, l_C is the center position of the LVDT, l is the core position deviating from the center position, α is the temperature coefficient, ΔT is the temperature deviation from the room temperature of 25 °C, and ϕ_S denotes the phase shift between the primary winding signal and the secondary winding signals. The LVDT output signal v_d is the difference between the two secondary winding signals v_{S1} and v_{S2} and can be expressed as

$$v_d = v_{S1} - v_{S2} = 2K_L l (1 - \alpha\Delta T) V_P \sin(\omega_{ex} t + \phi_S). \tag{2}$$

It can be seen that the amplitude of the LVDT signal v_d in Eq. (2) is proportional to the core position l and the variation in ambient temperature, ΔT. From Fig. 1(a), the sum voltage v_{sum} can be stated as

$$v_{sum} = -(v_{S1} + v_{S2}) = -K_S (1 - \alpha\Delta T) V_P \sin(\omega_{ex} t + \phi_S), \tag{3}$$

where $K_S = 2K_L l_C$. Note that the signals v_d and v_{sum} are 180° out of phase. The signal v_{sum} in Eq. (3) is directly proportional to the change in ambient temperature without the core displacement l.

To compensate for the temperature effect, the positive-peak amplitude of the signal v_{sum} is converted to the dc voltage v_a and compared with the reference voltage v_{ref} as shown in Fig. 1(a). The operation of the proposed technique is based on the assumption that the period of the excitation frequency is much less than the change in ambient temperature. The peak-amplitude finder provides the control signal for two SHCs to sample the positive-peak amplitudes of the signals v_{sum} and v_d to the signal v_a and the displacement signal v_{dl}, respectively. The voltage v_a is attenuated by the attenuator K_f to provide the signal v_f as the feedback signal. From Fig. 1(a), the reference voltage v_{ref} and the voltage v_f are provided for the difference and sum to obtain the signal v_m for the voltage-controlled amplifier A_{mul}. For steady-state operation, the voltage v_f is forced to equal the reference voltage v_{ref}. The signal v_{sin} is scaled by the signal v_m to provide the excitation signal v_{ex} for the LVDT. The signal v_{err} is the difference between the signals v_{ref} and v_f, which is processed by the block diagram K_1, to add with the reference voltage v_{ref}. The relationship of the signals v_m, v_{ref}, and v_f can be expressed as

$$v_m = v_{ref} + K_1(v_{ref} - v_f). \tag{4}$$

From Fig. 1(a), the signal v_{sin} is provided with constant amplitude and frequency. The diagram in Fig. 1(a) with the temperature effect can be simplified as shown in Fig. 1(b), where K_m is the voltage gain of the voltage-controlled amplifier A_{mul} and $\alpha_a = \alpha K_S$. The signal v_a against the reference voltage v_{ref} and the variation in ambient temperature ΔT can be stated as

$$v_a = \frac{K_m K_S (1 + K_1)}{1 + K_1 K_f K_m K_S} v_{ref} - \frac{\alpha_a}{1 + K_1 K_f K_m K_S} \Delta T. \tag{5}$$

If the gain K_f in Eq. (5) is assigned to equal $1/K_m K_S$, then the signal v_a can be expressed as

$$v_a = K_m K_S v_{ref} - \frac{\alpha_a}{1 + K_1} \Delta T. \tag{6}$$

For the proposed technique, the block diagram K_1 is replaced by the integrating amplifier. Therefore, the signal v_{err} of the difference and sum with integral action can be expressed as

$$v_{err}(s) = v_{ref}(s) - \frac{v_{ref}(s) - v_f(s)}{T_I s}, \tag{7}$$

where T_I denotes the integral time of the integrating amplifier. Therefore, the voltage v_a in Eq. (6) can be rewritten as

$$v_a(s) = K_m K_S v_{ref}(s) - \frac{\alpha_a T_I s}{(1 + T_I s)} \Delta T(s). \tag{8}$$

The circuit diagram of the proposed technique in Fig. 1(b) is shown in Fig. 2. The operation

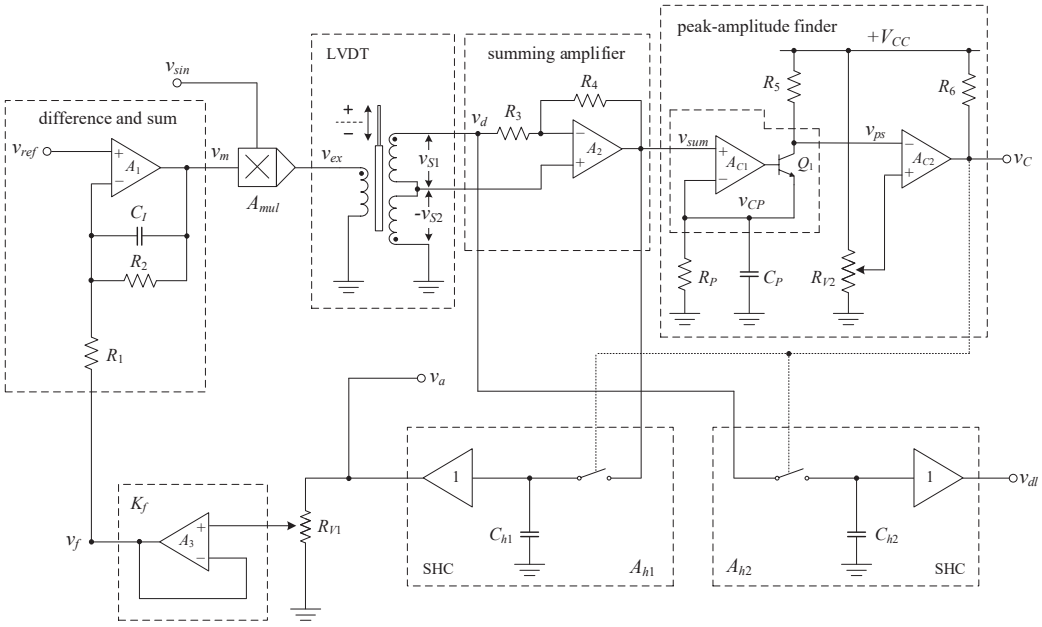

Fig. 2. Circuit of proposed technique.

of the proposed circuit in Fig. 2 can be explained as follows. The LVDT output signal v_d and the signal v_{S2} are summed using the summing amplifier formed by the opamp A_2 and the resistors R_3 and R_4 to provide the signal v_{sum}.[8] The peak-amplitude position of the signal v_{sum} is detected by the peak-amplitude finder that consists of the comparators A_{C1} and A_{C2}, the transistor Q_1, the capacitance C_P, the variable resistor R_{V2}, and the resistors R_P, R_5, and R_6. The peak-amplitude finder generates the control signal v_C in the form of narrow pulse that forces the SHCs A_{h1} and A_{h2} to sample the peak amplitudes of the signals v_{sum} and v_d to the voltages v_a and v_{dl}, respectively. The sampled signal v_a is attenuated by the variable resistor R_{V1} and the opamp A_3 to provide the feedback voltage $v_f = K_f v_a$. At room temperature (25 °C), the feedback signal v_f is equal to the reference voltage v_{ref}. The opamp A_1, the capacitance C_I, and the resistances R_1 and R_2 form the difference and sum with integral action. The resistance R_2 is provided to prevent the unstable operation of the opamp A_1 due to its parasitic capacitances. The output voltage v_m of the opamp A_1 can be given by

$$v_m(s) = \frac{(R_1 + R_2)}{R_1} \frac{\left[\frac{R_1 R_2}{(R_1 + R_2)} C_I s + 1\right]}{(R_2 C_I s + 1)} v_{ref}(s) - \frac{R_2}{R_1 (R_2 C_I s + 1)} v_f(s). \tag{9}$$

Practically, the resistance R_2 is assigned to be much greater than the resistance R_1. Thus, Eq. (9) can be approximated for $\omega > 0$ as

$$v_m(s) = \frac{(R_1 C_I s + 1)}{R_1 C_I s} v_{ref}(s) - \frac{1}{R_1 C_I s} v_f(s). \tag{10}$$

The voltage v_m is fed to the voltage-controlled amplifier A_{mul} to scale the amplitude of the signal v_{sin}. Therefore, the signal v_a of the proposed circuit in Fig. 2 can be stated as

$$v_a(s) = K_m K_S v_{ref}(s) - \frac{\alpha_a R_1 C_I s}{(1 + R_1 C_I s)} \Delta T(s). \tag{11}$$

From Eqs. (8) and (11), the integral time T_I is equal to $R_1 C_I$. It can be seen that the first term on the right-hand side of Eq. (11) exhibits the sensitivity of the LVDT without interference by the proposed feedback technique. The proportional-plus-integral action occurs only in the second term on the right-hand side of Eq. (11). It can be seen that the effect of the variation in ambient temperature ΔT is eliminated by the integral action. In addition, the core position l can be extracted from the positive-peak amplitude of the LVDT output signal v_d in the form of the displacement signal v_{dl} by using the SHC A_{h2}.[8] Therefore, the temperature effect in the displacement signal v_{dl} is also avoided.

3. Circuit Analysis

The ideal performance of the proposed circuit can be disturbed by the nonideal characteristic of devices used in the proposed scheme and the sampling rate of the SHC. The circuit analysis of the proposed scheme can be explained as follows. For the peak amplitude finder, the control signal v_C can be discontinued by the inappropriate value of the time constant $T_P = R_P C_P$. To prevent the discontinued pulse of the control signal v_C, the time constant T_P is assigned as $(T_{ex} - T_q)$, where T_{ex} and T_q denote the period of the excitation frequency and the acquisition time of the SHC, respectively. From Fig. 2, the positive-peak amplitude of the voltage v_{sum} is equal to $K_S V_P$. The voltage v_{CP} is fallen to the voltage $K_S V_P \sin[(1/2)\pi - (2\pi T_q/T_{ex})]$ in the period of $(T_{ex} - T_q)$ after the peak-amplitude position of the voltage v_{sum}. Thus, the time constant T_P can be stated as

$$T_P = R_P C_P = \frac{T_{ex} - T_q}{\ln \dfrac{1}{\sin\left(\dfrac{T_{ex} - 4T_q}{2T_{ex}}\right)\pi}}. \tag{12}$$

To minimize the ripple voltage of the SHC output, the pulse width of the control signal v_C is set to equal the acquisition time T_q of the SHC and provided by the time constant $T_W = R_5 C_P$. From Fig. 2, the resistor R_5 is used to convert the collector current i_{C1} of the transistor Q_1 to the voltage signal v_{ps}. The comparator A_{C2} and the variable resistor R_{V2} are provided for shaping the signal v_{ps} to the control signal v_C. The collector current i_{C1} of the transistor Q_1 is allowed to flow through the capacitor C_P and the resistor R_P, which can be expressed as

$$i_{C1} = \frac{V_{OP}\left[1 - \sin\left(\dfrac{T_{ex} - 4T_q}{2T_{ex}}\right)\right] C_P}{T_q}, \tag{13}$$

where V_{OP} denotes the peak amplitude of the voltage signal v_{sum}. The voltage across the resistor R_5 is equal to $i_{C1}R_5$ or $(V_{CC} - V_{OP})$. Therefore, the relationship of the time constants T_W and T_q can be given by

$$T_W = R_5 C_P = \frac{(V_{CC} - V_{OP})\, T_q}{V_{OP}\left[1 - \sin\left(\frac{T_{ex} - 4T_q}{2T_{ex}}\right)\pi\right]}. \tag{14}$$

If T_q = 6.5 μs, f_{ex} = 5 kHz, V_{OP} = 2.92 V, V_{CC} = 12 V, and C_P = 0.1 μF, then the resistances R_P and R_5 can be calculated as 92.16 and 9.7 kΩ, respectively. For stability consideration, the transfer function $F_{SH}(s)$ of the SHC can be approximated using the first-order Padé approximation for the sampling time T_{ex} as[17]

$$F_{SH}(s) = \frac{e^{-T_{ex}s}}{(1 + T_{SH}s)} = \frac{\left(-\frac{T_{ex}}{2}s + 1\right)}{\left(\frac{T_{ex}}{2}s + 1\right)(T_{SH}s + 1)}, \tag{15}$$

where T_{SH} and T_{ex} denote the response time of the SHC and the period of excitation frequency, respectively. Figure 3 shows a block diagram of Fig. 2 including the nonideal characteristics of active devices used in the proposed scheme. From Fig. 3, T_{su} and T_m are time constants of the opamp A_2 with unity gain and the response time of voltage-controlled amplifier A_{mul}, respectively. The time constant T_{su} of the opamp A_2 is equal to 1/*GBP*, where *GBP* is the gain bandwidth product of the opamp A_2. Note that the time constants T_{su}, T_m, and T_{SH} are much less than the period of the excitation frequency. Therefore, the transfer function of the proposed scheme in Fig. 3 can be approximated as

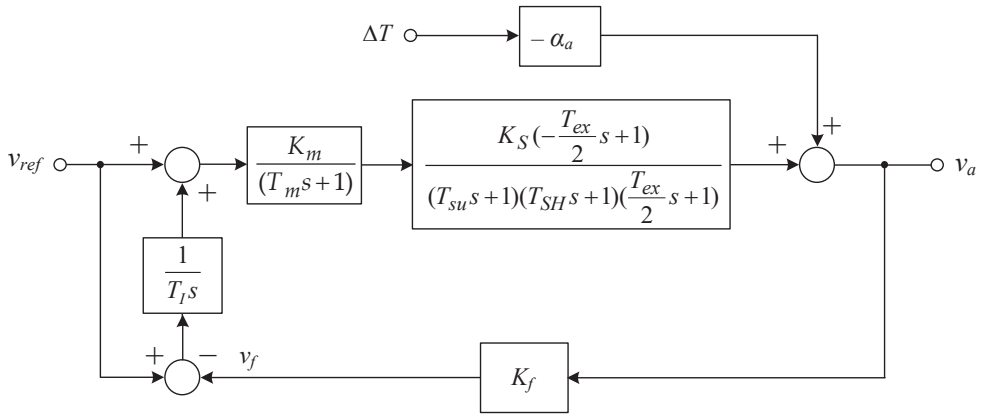

Fig. 3. Block diagram of Fig. 2.

$$v_a(s) = \frac{\left[\left(T_I - \frac{T_{ex}}{2}\right)s + 1\right]K_m K_S}{(T_I - \frac{K_m K_S K_f T_{ex}}{2})s + K_m K_S K_f} v_{ref}(s) - \frac{\alpha_a T_I s\left[\left(T_m + T_{su} - \frac{T_{ex}}{2}\right)s + 1\right]}{(T_I - \frac{K_m K_S K_f T_{ex}}{2})s + K_m K_S K_f}\Delta T(s). \tag{16}$$

Practically, the feedback gain K_f is assigned as $1/K_m K_S$. Also, the degree of change in ambient temperature is much lower than the excitation frequency. Then, the zeros of the second term on the right-hand side of Eq. (16) satisfy the condition of $|(T_m + T_{su} - T_{ex}/2)\omega| << 1$ and Eq. (16) can be approximately given by

$$v_a(s) = \frac{\left[\left(T_I - \frac{T_{ex}}{2}\right)s + 1\right]K_m K_S}{\left(T_I - \frac{T_{ex}}{2}\right)s + 1} v_{ref}(s) - \frac{\alpha_a T_I s}{\left(T_I - \frac{T_{ex}}{2}\right)s + 1}\Delta T(s). \tag{17}$$

From Eq. (17), the condition of $T_I > T_{ex}/2$ is assigned for stability consideration. The steady-state behavior against the signal v_{ref} for $K_m = 1$ can be given by

$$v_a = K_S v_{ref} = 2K_L l_C v_{ref}. \tag{18}$$

It can be seen that the amplitude of the signal v_a is only dependent on the sensitivity of the LVDT. If the change in ambient temperature, ΔT, is considered, then the derivation of the signal v_a against the temperature ΔT can be written as

$$v_a(s) = \frac{\alpha_a T_I s}{\left(T_I - \frac{T_{ex}}{2}\right)s + 1}\Delta T(s). \tag{19}$$

Practically, the change in ambient temperature, ΔT, is slow against the excitation frequency, and the time constant T_I is much larger than the period T_{ex} of the excitation frequency f_{ex} to prevent the phase shift caused by the sampling signal of the SHC. Therefore, Eq. (19) can be approximated as

$$v_a(s) = \frac{\alpha_a T_I s}{T_I s + 1}\Delta T(s). \tag{20}$$

The integral time T_I can be determined as $T_I \geq 10T_{ex}$. From the circuit in Fig. 2, the settling time T_S for the sudden change in ambient temperature, ΔT, can be measured from the interval time of the maximum change in the signal v_a to decrease to 0.1% and can be given by

$$T_S = 6.908T_I. \tag{21}$$

Practically, the integral time T_I is assigned as $10T_{ex}$ for the fast response time. Then, the settling time T_S is about 13.816 ms.

4. Experimental Results

The proposed circuit in Fig. 2 was implemented to confirm the circuit performance. The active devices used in the circuit were commercially available devices such as the opamp LF351 for A_1 and A_2, the voltage-controlled amplifier A_{mul} formed by the analog multiplier AD633, the SHC LF398 for A_{h1} and A_{h2}, and the comparator LM339 for A_{C2}. The comparator A_{C1} and the transistor Q_1 were provided in the same integrated circuit package as LM311. The GBPs of the opamps A_1 and A_2 are about 3 MHz and the time constant T_{su} can be approximated as 53 ns. The LVDT of ±12.5 mm stroke range and the sensitivity of 69 mV/mm/V at 5 kHz were used in this study.[8] The voltage gain K_m of the voltage-controlled amplifier A_{mul} was set to 1. The resistors $R_3 = R_4 = 30$ kΩ and $R_{V1} = R_{V2} = 10$ kΩ were assigned. The supply voltages were set to ±12 V. The excitation signal v_{sin} was assigned as a 5 kHz sinusoidal wave of 2 V peak-to-peak voltage, where the period T_{ex} of the excitation frequency was calculated as 0.2 ms. The reference voltage v_{ref} was set to 1 V. The capacitances $C_{h1} = C_{h2} = 0.01$ μF were used for the SHCs A_{h1} and A_{h2}, which caused the acquisition time of about $T_q = 6.5$ μs. For the peak amplitude finder, the capacitance C_P was chosen as 0.1 μF. Therefore, the resistances R_P and R_5 were determined from Eqs. (12) and (14) as 92.16 and 9.73 kΩ, respectively. From Eq. (21), the integral time T_I was assigned to equal $10T_{ex}$ or 2 ms for the fast response time and the resistor $R_1 = 20$ kΩ was calculated for the capacitance C_I set to 0.1 μF. The resistance $R_2 = 300$ kΩ was assigned for the condition of $R_2 >> R_1$ to avoid the unstable operation of the opamp A_1. The variable resistor R_{V1} was adjusted for scaling the voltage v_f equal to the reference voltage v_{ref} at room temperature. Figure 4 shows the signal waveforms v_{ex} and v_{sum} of the proposed scheme in Fig. 2. It also shows the phase shift between the signals v_{ex} and v_{sum} of about 18°. The output

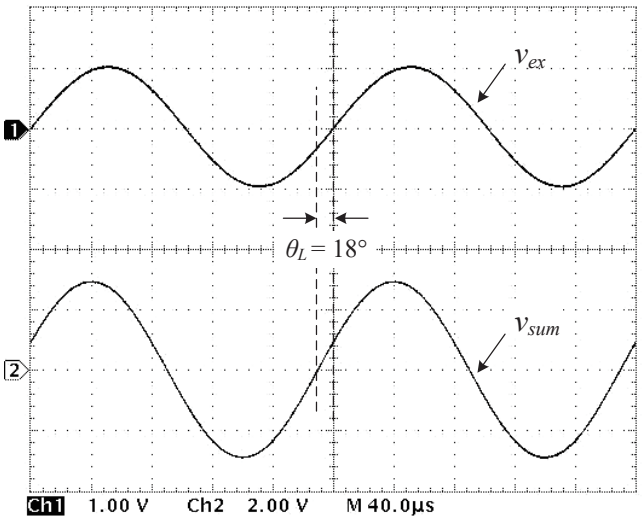

Fig. 4. Measured waveforms of v_{ex} and v_{sum}.

voltage v_a of the SHC A_{h1} is equal to the peak amplitude of the signal v_{sum} because the sampling signal v_C occurred at the peak-amplitude position of the signal v_{sum}. To verify the temperature performance, the LVDT was operated under the varying ambient temperature from 20 to 70 °C and the varying core position of the LVDT from −10 to 10 mm. The relative error of the measured results in percentage can be expressed as

$$relative\ error(\%) = \frac{|\Delta l|}{l} \times 100\%, \tag{22}$$

where Δl denotes the error between the measured and actual values. The temperature effect in the core displacement signal v_d without temperature compensation is shown in Fig. 5(a). Figure 5(b) shows the measured results of the core displacement signal with the temperature compensation. It can be seen that the proposed technique can reduce the maximum relative error from 6.52 to 0.098%. Figure 6 shows the drift of the offset voltage of the output signal v_{dl}

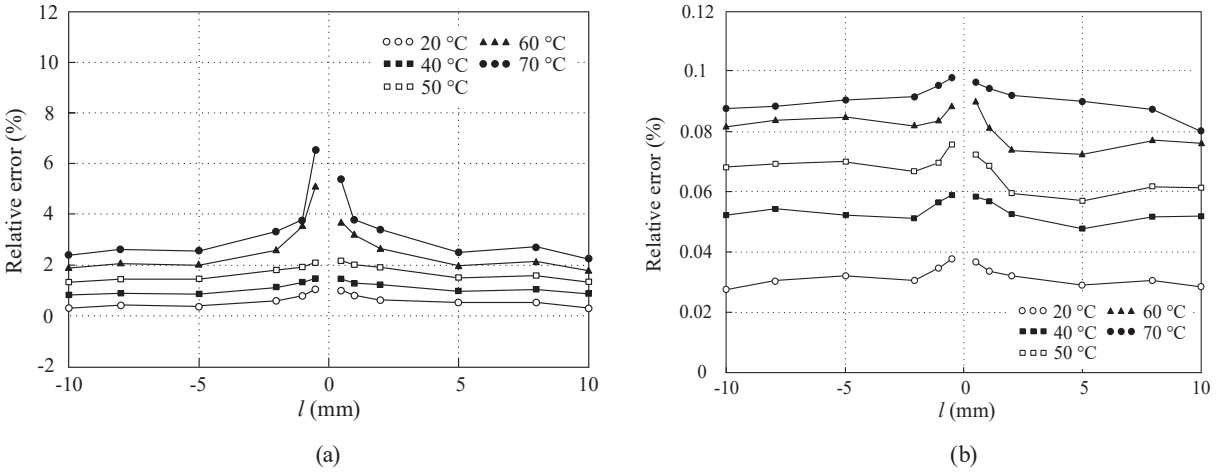

Fig. 5. Measured results. (a) Without temperature compensation and (b) proposed technique.

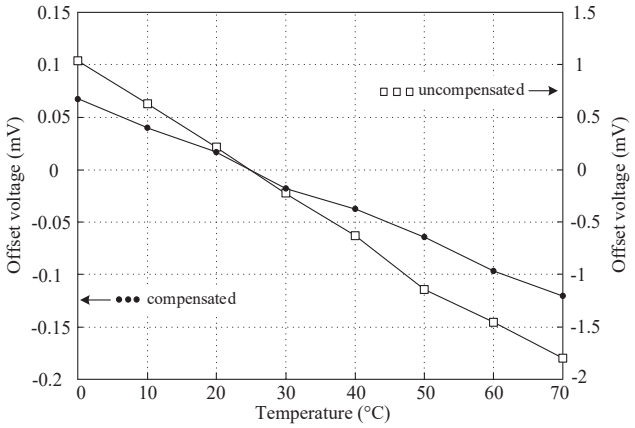

Fig. 6. Offset voltage against variation in ambient temperature.

against the variation in ambient temperature from 0 to 70 °C at the core position of 0 mm. From Fig. 6, the maximum drift of the offset voltage of about −0.12 mV is observed.

5. Conclusions

A technique to reduce the error of the LVDT signal caused by the variation in ambient temperature has been proposed. The effect of the change in ambient temperature was discussed in detail. The proposed technique required the integral action to reduce the error caused by the change in ambient temperature. The proposed circuit was implemented using commercially available devices. The performance characteristics of the proposed circuit were discussed and confirmed by experimental implementation. It is evident that the proposed scheme provides adequate performance for the applications of the LVDT in an environment with a highly fluctuating temperature such as a steam control valve, a power turbine, a nuclear reactor, a flight control actuation system, a variable area nozzle for aircraft, and an automotive active suspension system.

Acknowledgments

This work was supported by the King Mongkut's Institute of Technology Ladkrabang (KMITL), Thailand, under Grant No. KREF115701.

References

1 R. Pallas-Areny and J. G. Webster: Sensor and Signal Condition (Wiley, New York, 2001) p. 229.
2 S. Cetinkunt: Mechatronics (Wiley, New York, 2006) p. 227.
3 S. Lee and W. Kim: IEEE Trans. Control Syst. Technol. **18** (2010) 859.
4 M. Felix, A. Lizarraga, A. Islas, and A. Gonzales: 36th Conf. IEEE Industrial Electronics Society (IECON, 2010) 1769–1772.
5 G. Chen, B. Zhang, P. Liu, and H. Ding: IEEE Sensors J. **15** (2015) 2248.
6 J. Lee, K. C. Lee, S. Cho, and S. H. Sim: Sensors **17** (2017) 2317.
7 W. Petchmaneelumka, K. Songsuwankit, A. Rerkratn, and V. Riewruja: 3rd Int. Conf. Control, Automation and Robotics (ICCAR 2017) 758–761.
8 W. Petchmaneelumka, K. Songsuwankit, and V. Riewruja: Int. Rev. Electr. Eng. **11** (2016) 340.
9 W. Petchmaneelumka, K. Songsuwankit, and V. Riewruja: 9th Int. Conf. Computer and Automation Engineering (ICCAE 2017) 193–197.
10 A. Drumea, A. Vasile, M. Comes, and M. Blejan: 1st Electronic Systemintegration Technology Conf. (ESTC 2006) 629–634.
11 R. Casanella, O. Casas, and R. Pallas-Areny: Meas. Sci. Tech. **16** (2005) 1637.
12 C. S. Koukourlis, V. K. Trigonidis, and J. N. Sahalos: IEEE Trans. Instrum. Meas. **42** (1993) 926.
13 D. A. Johns and K. Martin: Analog Integrated Circuit Design (Wiley, New York, 1997) p. 389.
14 K. Ara: IEEE Trans. Instrum. Meas. **IM-21** (1972) 249.
15 S. C. Saxena and S. B. L. Se*ks*ena: IEEE Trans. Instrum. Meas. **38** (1989) 748.
16 T. S. Smith: U.S. Patent US 5087866 A (1991).
17 F. Golnaraghi and B. C. Kuo: Automatic Control System (Wiley, New York, 2010) p. 206.